A hybrid modeling environment to describe aggregates of cells heterogeneous for genotype and behavior with possible phenotypic transitions

A hybrid modeling environment to describe aggregates of cells heterogeneous for genotype and behavior with possible phenotypic transitions

Giulia Chiari[a,b,1], Marcello Edoardo Delitala[a,2], David Morselli[a,b,c,3], Marco Scianna[a,4]

[a] *Department of Mathematical Sciences "G. L. Lagrange", Politecnico di Torino, Corso Duca degli Abruzzi 24, 10129 Torino, Italy*
[b] *Department of Mathematics "G. Peano", Università di Torino, Via Carlo Alberto 10, 10124 Torino, Italy*
[c] *Department of Mathematics, School of Science, Computing and Engineering Technologies, Swinburne University of Technology, John St, 3122, Hawthorne, VIC, Australia*

Abstract

Biological systems are typically composed of cells heterogeneous for genotype and phenotype, the latter being time-evolving in response to internal or external stimuli. In order to take these aspects into account, we here propose a modeling framework in which a discrete structuring variable distuinguishes cells according to their genotype while a specific mathematical representation (i.e., individual/pointwise vs. collective/density-based) is assigned to each individual on the basis of its phenotypic hallmarks. A coherent procedure is then set to reproduce mechanisms of phenotypic plasticity: based on the definition of a bubble function, which gives the spatial distribution of the mass of a single cell, it possibly accounts the role played by stochasticity and environmental conditions. The proposed modeling environment is then enriched with the inclusion of further cell behavior, such as migratory dynamics and duplication/apoptotic processes, as well as with chemical kinetics. The resulting multiscale hybrid approach is finally applied to the scenario of a heterogeneous tumor aggregate cultured *in vitro*.

Keywords: heterogeneous cell population, phenotypic plasticity, hybrid model, discrete vs. continuous mathematical descriptions
37N25, 45J05, 92C17

[1] giulia.chiari@polito.it
[2] marcello.delitala@polito.it
[3] david.morselli@polito.it
[4] marco.scianna@polito.it

1. Introduction

We here propose a theoretical/computational approach that allows to characterize cells both at the *genotypic* and at the *phenotypic* level. In particular, a *discrete trait variable* is used to structure a cell population with respect to individual genetic makeup. In other words, each value of this variable is set to correspond to a given sequence of genes. A distinct *mathematical representation*, i.e., pointwise/discrete or density-based/continuous, is instead employed to distinguish cells with respect to their (possibly dicothomic) phenotype/effective behavior, which is established by gene transcription and therefore expression levels. In this respect, the subpopulation of cells with a given phenotype is represented by a set of particles, whereas the remaining group of individuals, characterized by the alternative phenotype, is represented by a continuous density function.

The association between a cell phenotype and a mathematical representation is here determined by reasonable biological arguments. A pointwise description is in fact more appropriate for *specialized/activated/highly metabolic* cells or for cells with *mesenchymal* determinants, i.e., with the ability to undergo individual directional movement in response to environmental cues. On the other hand, a density-based representation, characterized by a lower level of individual detail, is more suitable for *non-specialized/quiescent/poorly metabolic* cell ensembles or for cells with *epithelial* determinants, i.e., which undergo collective dynamics mainly guided by intercellular communication.

In our model, the "discrete vs. continuous" dichotomy is indeed not referred to the spatial scale at which the system is modeled (i.e., "microscopic vs. macroscopic"); rather it is employed to differentiate cell behavior. This aspect distinguishes the mathematical environment proposed here from classical approaches presented in the literature, which typically rely on the idea that a density-based description is a good approximation of the discrete counterpart in the case of systems composed of substantially high amounts of particles with negligible mass. These mathematical frameworks are typically based on mean-field limits [1], heuristic laws of large numbers [2], or coarse-graining procedures [3]. Macroscopic formulations have been also derived by selected lattice-gas cellular automata (LGCA) in [4].

By the definition of a bubble function that represents a plausible spatial distribution of the mass of a single individual, we then implement the passage between the two descriptive instances. This strategy, firstly proposed in [5, 6], allows to model the phenomenon of *phenotypic plasticity*, that is the ability of cells to switch back and forth among multiple phenotypes while maintaining unaltered their genotype [7]. In particular, we here assume that phenotypic conversions are triggered by environmental signals, dependent on cell genetic traits, and affected by randomness. The inclusion of the last aspect represents a significant novelty w.r.t. the previously-cited works [5, 6]. The possibility for cells to have an evolving phenotype has been taken into account in some other approaches. For instance, in individual-based/cellular automata models, each single cell is allowed to vary the label indicating its actual phenotype, as in the

case of the well-celebrated Cellular Potts Model, see [8] and reference therein. Also a hybrid approach allows the description of different phenotypes with different discrete populations, as done in [9]; differently from the modeling approach we present, in this context the discrete setting is used for all cell dynamics while the continuous description is adopted for microenvironmental dynamics, such as oxygen or extracellular matrix. Models based on a continuous cell description (also in the framework of the Theory of Mixtures) instead typically associate to each subpopulation a distinct density function: phenotypic conversions are then implemented by mass exchanging terms included in the evolution equations for cell dynamics, as done for instance in [10, 11]. We refer to [12] for a comprehensive review of mathematical approaches to model cell plasticity in the framework of tumor growth. Finally, in approaches dealing with structured populations, where the trait variable is not referred to the genotype of cells but rather to their behavioral determinants, and therefore takes values in a continuous interval, random phenotypic transitions are accounted by including a diffusion term on the trait domain, see, e.g., [13, 14, 15]. However, in all these cases phenotypic switches do not imply variations in the mathematical representation of cells, which is a novelty introduced in the above-cited works [5, 6] and here extended by the inclusion of genetic traits and probabilistic aspects.

Our model is finally enriched with cell migratory and growth dynamics, that are assumed to depend on cell genotype and phenotype.

Applicative potential of the proposed model. The proposed modeling approach is indeed able to capture and represent genetic and phenotypic heterogeneity among a given system of cells, as well as selected mechanisms underlying phenotypic plasticity. Its possible applications therefore span a wide spectrum of phenomena since the evolution of aggregates of cells, from small clusters to large populations, is typically determined by cooperative dynamics and interactions between the component individuals differing both at the DNA and at the protein level.

For instance, in most collective cell movement, few specialized individuals, able to sense environmental chemical signals, typically behave as a patterning guidance for the rest of the system, which instead passively displaces only due to adhesion, see [16, 17] and references therein. It is the case of angiogenic processes, where a small number of endothelial cells forming the walls of pre-existing vessels acquire a leader/tip phenotype, representing migratory cues for the neighboring individuals with a follower/stalk behavior [18]. These mechanisms are triggered by a number of diffusing growth factors (e.g., vascular endothelial growth factor - VEGF, hepatocyte growth factors - HGF) and mediated by the well-known Delta-Notch signaling pathways [19, 20].

Similarly, during skin repair after injury, the cells located at the front of the epidermal monolayers that invade the wounded region are characterized by actin-rich lamellipodia and pseudopodia, that allow active movement, and are able to synthesize a new basement membrane, whereas individuals at the rear regions only passively displace dragged by cell–cell adhesive interactions.

Cell heterogeneity is also observed in pathological situations, such as in tu-

mor growth. For instance, individuals exhibiting different sequences of genes and/or phenotypic determinants have been found in several types of disease, including breast cancer [21], colorectal cancer [22], brain cancer [23], and prostate cancer [24]. Interestingly, it has been shown that malignant cells within the same mass exhibit different behavior in spite of carrying the same genetic alterations [25]. Cancer cells have been also demonstrated to be able to switch between alternative phenotypic states either spontaneously or in response to ecological inputs. For example, nutrient-deprived malignant individuals activate downstream pathways that result in a shift towards a more aggressive behavior. These cells in fact lose epithelial characteristics, such as high adhesiveness and high duplication capacity, and acquire mesenchymal features, such as enhanced motility, which allow them to more effectively invade surrounding tissue. This phenomenon, denoted as *epithelial-to-mesenchimal transition (EMT)*, is also involved in physiological scenarios, such as morphogenesis and organogenesis. The inverse process may occur as well: tumor cell with mesenchymal determinants can lose their migratory freedom and re-acquire epithelial hallmarks, including expression of junctional proteins, when experiencing a sufficient level of environmental substrates [26]. Phenotypic differentiation and conversions of genetically identical tumor cells have been also shown to (i) facilitate survival and adaptation of the entire disease, which can play "hide-and-seek" with multiple therapeutic regimes [27, 28], and (ii) fuel subsequent genetic evolution [29, 30].

Structure of the article. The remaining part of the article is organized as follows. In Section 2, we introduce the main model ingredients and present a sample numerical realization that shows how the procedure for the phenotypic switch works. In Section 3, we apply our approach to the representative case of a heterogeneous tumor aggregate evolving in an oxygen-deprived domain. In Section 4, we finally give some conclusive remarks and hints for further model developments.

2. Proposed approach and representative simulation

We are interested in modeling the evolution of an aggregate of cells within a closed two-dimensional domain $D \subset \mathbb{R}^2$, whose dynamics are studied for the period $T = [0, t_{\mathrm{F}}] \subset \mathbb{R}_0^+$, t being the time variable. The spatial domain D may reproduce, for instance, a planar section of an *in vivo* tissue or the surface of a *Petri dish*, usually employed in experimental studies.

The cells composing the system are here differentiated according to two determinants, as sketched in Fig. 1 (A):

- their *genotype*, by the use of a *discrete trait variable* u;
- their *phenotype*, by the use of different *mathematical representations*.

Our approach is indeed based on the assumption that there is not a deterministic and/or necessary relation between the genetic trait of a cell and its phenotype:

the latter is in fact determined at the protein level, i.e., by effective gene transcription and expression levels, which are eventually affected by stochasticity and extracellular/environmental stimuli and conditions (by the so-called surrounding *ecology*).

The structuring variable u is set to assume a given number of values, say K, i.e., $u \in U = \{u_k\}_{k=1}^{K}$. In this respect, the generic state $u_{\hat{k}}$ defines the cell clone characterized by the $\hat{k}$-th genetic makeup, i.e., by the $\hat{k}$-th sequence of genes.

We then consider two alternative cell phenotypes, say "A" and "B", and associate each of them to a distinct mathematical descriptive instance, as proposed in [5, 6]. In particular, for a given cell variant with genotipic trait $u_{\hat{k}} \in U$, the individuals that show phenotype A have a *discrete* representation: they are reproduced with dimensionless points with concentrated unitary mass and identified by their actual position in space (see panel (A) in Fig. 1). Such subgroup of agents can be indeed collected in the following set:

$$\boldsymbol{X}^{\mathrm{A}}_{u_{\hat{k}}}(t) = \left\{ \boldsymbol{x}_{1,u_{\hat{k}}}(t), \ldots, \boldsymbol{x}_{N^{\mathrm{A}}_{u_{\hat{k}}}(t),u_{\hat{k}}}(t) \right\}, \tag{1}$$

with $\boldsymbol{x}_{i,u_{\hat{k}}}(t) \in D$, for $i = 1, ..., N^{\mathrm{A}}_{u_{\hat{k}}}(t)$, being $N^{\mathrm{A}}_{u_{\hat{k}}}(t)$ the number of cells with phenotype A and genotype $u_{\hat{k}}$ at time t. The overall amount of individuals with phenotype A within the entire aggregate can be therefore computed as

$$N^{\mathrm{A}}(t) = \sum_{k=1}^{K} N^{\mathrm{A}}_{u_k}(t). \tag{2}$$

The remaining part of the clone of cells with the $\hat{k}$-th genetic trait is instead characterized by phenotype B and *collectively* described by the number density function $a^{\mathrm{B}}(t, \boldsymbol{y}, u_{\hat{k}})\colon T \times D \times U \mapsto \mathbb{R}_0^+$ (as shown in Fig. 1 (A)). The local amount of individuals with phenotype B can be therefore evaluated as

$$\rho^{\mathrm{B}}(t, \boldsymbol{y}) = \sum_{k=1}^{K} a^{\mathrm{B}}(t, \boldsymbol{y}, u_k). \tag{3}$$

In this respect, $a^{\mathrm{B}}(t, \boldsymbol{y}, \cdot)$ can be interpreted as the local distribution of cells with phenotype B on the genotype space U. The overall number of agents with phenotype B actually present within the entire domain D can be then approximated by integrating ρ^{B} along the space variable and rounding down the obtained value:

$$N^{\mathrm{B}}(t) = \left\lfloor \int_D \rho^{\mathrm{B}}(t, \boldsymbol{y}) \, \mathrm{d}\boldsymbol{y} \right\rfloor. \tag{4}$$

The total number of cells composing the aggregate at any given time t is finally equal to $N(t) = N^{\mathrm{A}}(t) + N^{\mathrm{B}}(t)$.

Remarks. For the sake of completeness, we now give some comments on the above-proposed modeling framework:

- the association between the different cell genetic makeups and the corresponding values of the variable u is arbitrary;
- the association between a cell phenotype and the corresponding mathematical representation is instead suggested by biological considerations, as explained in the Introduction of this article;
- in principle, our approach could include more than two cell phenotypes. This would require the use of hybrid mathematical representations, i.e., able to account for a proper amount of microscopic granularity within a macroscopic/continuous description of the system of interest, which would be possible, for instance, by employing tools of Measure Theory [31, 32];
- the proposed modeling environment is *hybrid* but not, so far, multiscale, in the sense that different mathematical objects (i.e., material points and number densities) are used together but represent biological elements at the same spatial scale, i.e., different types of cells.

Modeling cell phenotypic plasticity. In a wide range of biological phenomena, cells are able to change phenotype while maintaining their genetic makeup, i.e., to vary the expression level of one or more of their genes. To reproduce this phenomenon in our modeling framework, we need to set up a procedure to switch between the two cell descriptive instances. It is indeed necessary to define a proper correspondence between the pointwise and the density-based representation of a single cell. In this respect, let us proceed as in [5, 6] and introduce a function $\varphi_{\boldsymbol{x}}(\boldsymbol{y}) : D \times D \mapsto \mathbb{R}_0^+$ such that:

$$\int_D \varphi_{\boldsymbol{x}}(\boldsymbol{y}) \, \mathrm{d}\boldsymbol{y} = 1. \tag{5}$$

$\varphi_{\boldsymbol{x}}$ approximates the spatial distribution of a cell whose center is located in $\boldsymbol{x} \in D$. In principle, there exist several possible options to explicit $\varphi_{\boldsymbol{x}}(\boldsymbol{y})$. However, in accordance with the already-cited works [5, 6], we hereafter use the following *bubble* function, which assumes a greater amount of cell mass around $\boldsymbol{x}$, as shown in Fig. 1 (B):

$$\varphi_{\boldsymbol{x}}(\boldsymbol{y}) = \begin{cases} \dfrac{4}{\pi r^8}(r^2 - |\boldsymbol{y} - \boldsymbol{x}|^2)^3, & \text{if } |\boldsymbol{y} - \boldsymbol{x}| \leq r; \\ 0, & \text{otherwise.} \end{cases} \tag{6}$$

In Eq. (6), $|\cdot|$ identifies the Euclidean norm while r is set to approximate a mean cell radius: hereafter, it will have a value of 15 μm.

Let us now assume that, at a certain time t, the i-th cell with phenotype A and genotype $u_{\hat{k}} \in U$ undergoes a transition to phenotype B. From a biological perspective, this may be the result of environmental stimuli (triggered by chemical signals or by intercellular communication) or of the fact that the individual i is able to maintain phenotype A only for a limited period of time (e.g., due to high metabolic costs). The proposed A-to-B phenotypic switch can be then

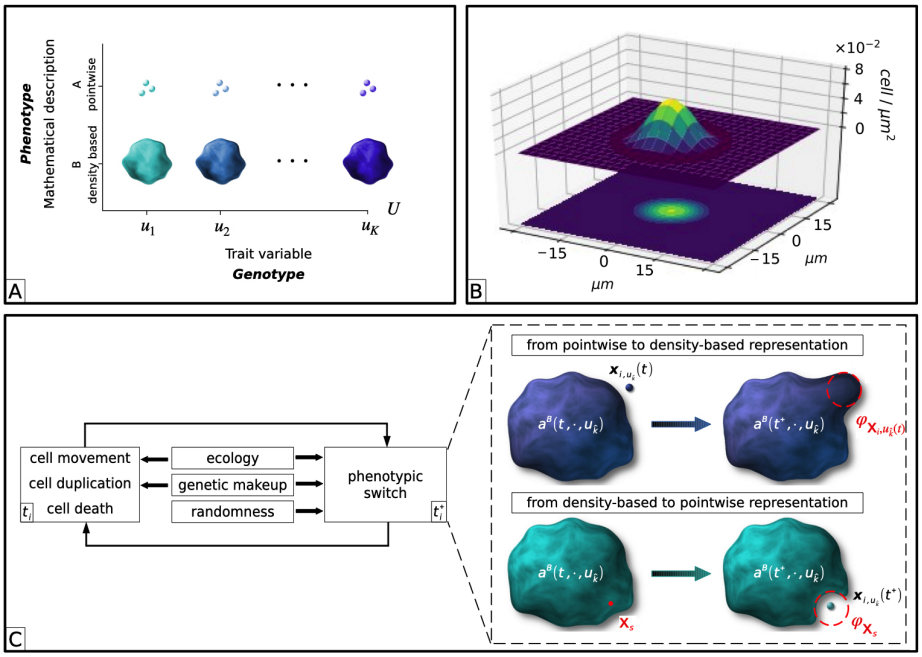

Figure 1: (A) In our modeling environment, each cell is differentiated for genotype, i.e., by the use of a discrete structuring variable $u \in U$, and for phenotype, i.e., by the use of a specific mathematical representation. In particular, we only consider two alternative individual phenotypes, which are set to correspond either to a pointwise or to a density-based descriptive instance. (B) For representative purposes, bidimensional and threedimensional plots of the bubble function centered in $\boldsymbol{x} = (0,0)$, i.e., $\varphi_{(0,0)}$ (cf. Eq. (6)). We recall that the radius r of the round support of φ is constantly taken equal to 15 μm. (C) We here set that cell dynamics such as growth, migration, and phenotypic switches are affected both by individual genetic trait and by variations in environmental (i.e., ecological) conditions. Stochasticity plays a role as well. In particular, A-to-B phenotypic transition of the generic cell i with genotype $u_{\hat{k}}$ is implemented by the removal of the material point located in $\boldsymbol{x}_{i,u_{\hat{k}}}$ and the simultaneous addition of the corresponding bubble function $\varphi_{\boldsymbol{x}_{i,u_{\hat{k}}}}$ to the mass distribution $a^{\mathrm{B}}(\cdot,\cdot,u_{\hat{k}})$. Conversely, a B-to-A phenotypic switch, stimulated in the domain point $\boldsymbol{x}_{\mathrm{s}}$ and involving the cell variant with genotype $u_{\hat{k}}$, amounts in the local creation of a new material point $\boldsymbol{x}_{N^{\mathrm{A}}_{u_{\hat{k}}}(t)+1,u_{\hat{k}}}$ and in the simultaneous removal of the bubble function $\varphi_{\boldsymbol{x}_{\mathrm{s}}}$ to the mass distribution $a^{\mathrm{B}}(\cdot,\cdot,u_{\hat{k}})$.

implemented in our modeling framework by removing the material point located in $\boldsymbol{x}_{i,u_{\hat{k}}}(t)$ and by simultaneously adding the equivalent mass function $\varphi_{\boldsymbol{x}_{i,u_{\hat{k}}}(t)}$ to the density of the cell variant characterized by the same trait $u_{\hat{k}}$, as shown in Fig. 1 (C). In mathematical terms, we indeed get the following relations:

$$\begin{cases} \boldsymbol{X}^{\mathrm{A}}_{u_{\hat{k}}}(t^+) = \boldsymbol{X}^{\mathrm{A}}_{u_{\hat{k}}}(t) \setminus \{\boldsymbol{x}_{i,u_{\hat{k}}}(t)\}; \\ \boldsymbol{X}^{\mathrm{A}}_{u_k}(t^+) = \boldsymbol{X}^{\mathrm{A}}_{u_k}(t), \quad \text{for all } k \neq \hat{k}; \\ a^{\mathrm{B}}(t^+,\boldsymbol{y},u_{\hat{k}}) = a^{\mathrm{B}}(t,\boldsymbol{y},u_{\hat{k}}) + \varphi_{\boldsymbol{x}_{i,u_{\hat{k}}}(t)}(\boldsymbol{y}), \quad \text{for all } \boldsymbol{y} \in D; \\ a^{\mathrm{B}}(t^+,\boldsymbol{y},u_k) = a^{\mathrm{B}}(t,\boldsymbol{y},u_k), \quad \text{for all } k \neq \hat{k}; \ \text{ and } \ \boldsymbol{y} \in D. \end{cases} \tag{7}$$

Finally, the remaining particles with phenotype A and genotype $u_{\hat{k}}$ are renumbered according to the rule

$$\boldsymbol{x}_{j,u_{\hat{k}}}(t^+) = \begin{cases} \boldsymbol{x}_{j,u_{\hat{k}}}(t), & \text{if } j < i; \\ \boldsymbol{x}_{j-1,u_{\hat{k}}}(t), & \text{if } j > i. \end{cases} \tag{8}$$

In Eqs. (7) and (8), as well as in the following, the notation t^+ is used to specify that, from a *numerical point of view*, phenotypic transitions are not simultaneously implemented with the other processes, e.g., cell movement, duplication, death, that occur at the same time instant (see also [5, 6]). The generalization of the above procedure to more cells that actually switch from phenotype A to phenotype B, possibly with different genotypic traits, is straightforward.

Let us then conversely assume that, at time t, an environmental stimulus, that is in principle able to trigger a transition from phenotype B to phenotype A in individuals with the generic genotype $u_{\hat{k}} \in U$, is active in a given domain location, say $\boldsymbol{x}_{\rm s} \in D$. Such a switch can occur only if there is a sufficient density of the cell variant of interest to have a localized agent placed in $\boldsymbol{x}_{\rm s}$. In mathematical terms, this amounts to satisfy the following local constraint:

$$a^{\rm B}(t, \boldsymbol{y}, u_{\hat{k}}) \geq \varphi_{\boldsymbol{x}_{\rm s}}(\boldsymbol{y}), \quad \text{for all } \boldsymbol{y} \in D. \tag{9}$$

In this case, the cell phenotypic transition from B to A (and the corresponding representation switch) results from the removal of $\varphi_{\boldsymbol{x}_{\rm s}}$ from the distribution $a^{\rm B}(t, \cdot, u_{\hat{k}})$, accompanied by the addition of the corresponding new element to the set $\mathbf{X}^{\rm A}_{u_{\hat{k}}}$ (see panel (C) in Fig. 1):

$$\begin{cases} \boldsymbol{X}^{\rm A}_{u_{\hat{k}}}(t^+) = \boldsymbol{X}^{\rm A}_{u_{\hat{k}}}(t) \cup \{\boldsymbol{x}_{N^{\rm A}_{u_{\hat{k}}}(t)+1,u_{\hat{k}}}(t) \equiv \boldsymbol{x}_{\rm s}\}; \\ \boldsymbol{X}^{\rm A}_{u_k}(t^+) = \boldsymbol{X}^{\rm A}_{u_k}(t), \quad \text{for all } k \neq \hat{k}; \\ a^{\rm B}(t^+, \boldsymbol{y}, u_{\hat{k}}) = a^{\rm B}(t, \boldsymbol{y}, u_{\hat{k}}) - \varphi_{\boldsymbol{x}_{\rm s}(t)}(\boldsymbol{y}), \quad \text{for all } \boldsymbol{y} \in D; \\ a^{\rm B}(t^+, \boldsymbol{y}, u_k) = a^{\rm B}(t, \boldsymbol{y}, u_k), \quad \text{for all } k \neq \hat{k} \text{ and } \boldsymbol{y} \in D. \end{cases} \tag{10}$$

Furthermore, the following rules are set:

- in the case of B-to-A phenotypic transitions involving the same cell clone, e..g, with genotype $u_{\hat{k}}$, and simultaneously stimulated in two distinct domain points $\boldsymbol{x}_{\rm s1}$ and $\boldsymbol{x}_{\rm s2}$ such that $\varphi_{\boldsymbol{x}_{\rm s1}}$ and $\varphi_{\boldsymbol{x}_{\rm s2}}$ overlap, two alternative options are accounted: (i) if $a^{\rm B}(t, \boldsymbol{y}, u_{\hat{k}}) \geq \varphi_{\boldsymbol{x}_{\rm s1}}(\boldsymbol{y}) + \varphi_{\boldsymbol{x}_{\rm s2}}(\boldsymbol{y})$ for any $\boldsymbol{y} \in D$, then both behavioral switches occur; (ii) if, otherwise, $a^{\rm B}(t, \boldsymbol{y}, u_{\hat{k}}) \geq \varphi_{\boldsymbol{x}_{\rm s1}}(\boldsymbol{y}), \varphi_{\boldsymbol{x}_{\rm s2}}(\boldsymbol{y})$ but $a^{\rm B}(t, \boldsymbol{y}, u_{\hat{k}}) < \varphi_{\boldsymbol{x}_{\rm s1}}(\boldsymbol{y}) + \varphi_{\boldsymbol{x}_{\rm s2}}(\boldsymbol{y})$ for at least one domain point, then only one transition takes place, which is randomly established. The same rule is extended in the case of more than two phenotypic transitions with analogous characteristics;

- B-to-A phenotypic transitions are not allowed in any domain point effectively occupied by a pointwise agent (regardless its genotype). Coherently,

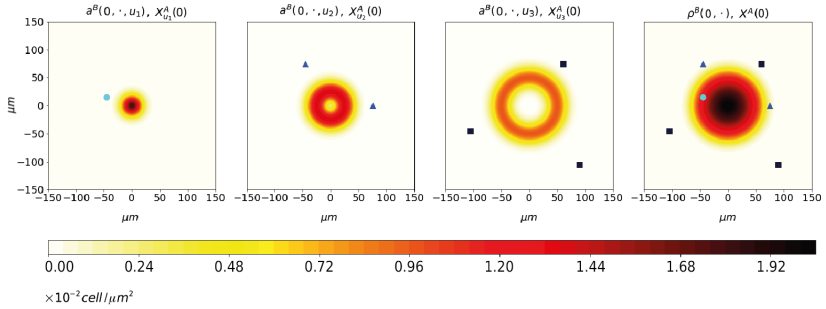

Figure 2: Initial condition of the representative simulation, as specified by Eq. (11). The subpopulation with phenotype B has a radial symmetry: in particular, the cell variant with genotype u_1 is mainly located at the bulk of the cluster, the cell variant with u_3 forms an external ring, whereas the cell variant with u_2 is distributed in the intermediate region. A group of individuals with phenotype A is then dispersed around and within the distribution of cells with phenotype B. In particular, we hereafter use light blue circles to indicate particles with phenotype A and genotype u_1, blue triangles to indicate particles with phenotype A and genotype u_2, and dark blue squares to indicate particles with phenotype A and genotype u_3. Such an initial cell configuration is maintained in the case of the model application proposed in Section 3.

only one B-to-A phenotypic switch is allowed (and arbitrarily established) at the same time in the same domain point. These constraints are consistent with the observation that, in a wide range of phenomena, a cell that activates inhibits the surrounding individuals to undergo the same process. It is the case, for instance, of the tip cell selection and lateral inhibition mechanism controlled by the Delta-Notch pathways during physio-pathological angiogenesis;

- simultaneous B-to-A phenotypic switches occurring at far enough spatial regions are instead always permitted.

It is instead useful to remark that the above ones are tailored rules and therefore can be in principle neglected and/or replaced by other assumptions.

Sample simulation. Before including in the proposed modeling framework more realistic biological mechanisms and dynamics, let us propose and comment a representative numerical realization. It deals with a colony of cells which do not grow or move but only undergo arbitrarily selected phenotypic transitions. In more details, in the spatial domain $D = [-150\ \mu\text{m}, 150\ \mu\text{m}]^2$, we place an aggregate whose component individuals can have three different genetic make-ups, i.e., $U = \{u_1, u_2, u_3\}$, while showing the usual dichotomy in the phenotype, i.e., A and B. The initial system configuration is then given by the following

distribution of cells:

$$\begin{cases} \boldsymbol{X}^{\mathrm{A}}_{u_1}(0) = \{\, \boldsymbol{x}_{1,u_1} = (-45, 15) \,\}; \\ \boldsymbol{X}^{\mathrm{A}}_{u_2}(0) = \{\, \boldsymbol{x}_{1,u_2} = (75, 0);\ \boldsymbol{x}_{2,u_2} = (-45, 75) \,\}; \\ \boldsymbol{X}^{\mathrm{A}}_{u_3}(0) = \{\, \boldsymbol{x}_{1,u_3} = (60, 75);\ \boldsymbol{x}_{2,u_3} = (90, -105);\ \boldsymbol{x}_{3,u_3} = (-105, -45) \,\}; \\ a^{\mathrm{B}}(0, \boldsymbol{y}, u_1) = 3.1\ m_\varphi\ \exp\Big(-\dfrac{|\boldsymbol{y}|^2}{325}\Big); \\ a^{\mathrm{B}}(0, \boldsymbol{y}, u_2) = 2.4\ m_\varphi\ \exp\Big(-\dfrac{|\boldsymbol{y} - 25|^2}{325}\Big); \\ a^{\mathrm{B}}(0, \boldsymbol{y}, u_3) = 1.7\ m_\varphi\ \exp\Big(-\dfrac{|\boldsymbol{y} - 50|^2}{325}\Big), \end{cases} \tag{11}$$

for all $\boldsymbol{y} \in D$, being $m_\varphi = 4/\pi r^8$ the maximum of the *bubble* function (cf. Eq. (6)), see Fig. 2. The overall number of cells at the onset of the simulation, which remains constant in time due to the absence of duplication/death mechanisms, amounts to:

$$\begin{aligned} N(0) &= N^{\mathrm{A}}(0) + N^{\mathrm{B}}(0) \\ &= [\boldsymbol{X}^{\mathrm{A}}_{u_1}(0)] + [\boldsymbol{X}^{\mathrm{A}}_{u_2}(0)] + [\boldsymbol{X}^{\mathrm{A}}_{u_3}(0)] + \left\lfloor \int_D \rho^{\mathrm{B}}(0, \boldsymbol{y})\, \mathrm{d}\boldsymbol{y} \right\rfloor \\ &= 6 + \left\lfloor \int_D [a^{\mathrm{B}}(0, \boldsymbol{y}, u_1) + a^{\mathrm{B}}(0, \boldsymbol{y}, u_2) + a^{\mathrm{B}}(0, \boldsymbol{y}, u_3)]\, \mathrm{d}\boldsymbol{y} \right\rfloor = 6 + 188 = 194, \end{aligned} \tag{12}$$

where $[Q]$ indicates the cardinality of a generic set Q.

At a given time t_1, an external input able to stimulate a switch from phenotype B to phenotype A for all cell clones, regardless their genetic trait, activates in an arbitrary set of domain points, radially disposed along the main axies: $\boldsymbol{x}_{\mathrm{s}1} = (15, 0)$, $\boldsymbol{x}_{\mathrm{s}2} = (50, 0)$, $\boldsymbol{x}_{\mathrm{s}3} = (85, 0)$, $\boldsymbol{x}_{\mathrm{s}4} = (0, 15)$, $\boldsymbol{x}_{\mathrm{s}5} = (0, 50)$, $\boldsymbol{x}_{\mathrm{s}6} = (0, 85)$, $\boldsymbol{x}_{\mathrm{s}7} = (-15, 0)$, $\boldsymbol{x}_{\mathrm{s}8} = (-50, 0)$, $\boldsymbol{x}_{\mathrm{s}9} = (-85, 0)$, $\boldsymbol{x}_{\mathrm{s}10} = (0, -15)$, $\boldsymbol{x}_{\mathrm{s}11} = (0, -50)$, and $\boldsymbol{x}_{\mathrm{s}12} = (0, -85)$, see top panels in Fig. 3. In this respect:

- no transition takes place in $\boldsymbol{x}_{\mathrm{s}3}$, $\boldsymbol{x}_{\mathrm{s}6}$, $\boldsymbol{x}_{\mathrm{s}9}$, and $\boldsymbol{x}_{\mathrm{s}12}$ due to the lack of sufficient mass density of any cell genetic variant;
- in $\boldsymbol{x}_{\mathrm{s}2}$, $\boldsymbol{x}_{\mathrm{s}5}$, $\boldsymbol{x}_{\mathrm{s}8}$, $\boldsymbol{x}_{\mathrm{s}11}$, only the subpolulation with genetic trait u_3 is able to undergoes phenotypic switch, as $a^{\mathrm{B}}(0, \boldsymbol{y}, u_3) \geq \varphi_{\boldsymbol{x}_{\mathrm{sj}}}(\boldsymbol{y})$ for all $\boldsymbol{y} \in D$ and sj $\in$ s2, s5, s8, s11, a condition that instead is not satisfied by the distributions of the other cell genotypes;
- in $\boldsymbol{x}_{\mathrm{s}1}$, $\boldsymbol{x}_{\mathrm{s}4}$, $\boldsymbol{x}_{\mathrm{s}7}$, $\boldsymbol{x}_{\mathrm{s}10}$, both the cell clone with genotype u_1 and the cell clone with genotype u_2 have in principle enough mass to undergo a single-cell switch from phenotype B to phenotype A (i.e., $a^{\mathrm{B}}(0, \boldsymbol{y}, u_1), a^{\mathrm{B}}(0, \boldsymbol{y}, u_2) \geq \varphi_{\boldsymbol{x}_{\mathrm{sj}}}(\boldsymbol{y})$ for all $\boldsymbol{y} \in D$ and sj $\in$ s1, s4, s7, s10). However, as previously commented, only a single B-to-A phenptypic switch is allowed to occur at a given time in a given domain location: in this respect, we arbitrarily establish that in each of the four points, only the genetic variant u_2 is subjected to phenotypic conversion.

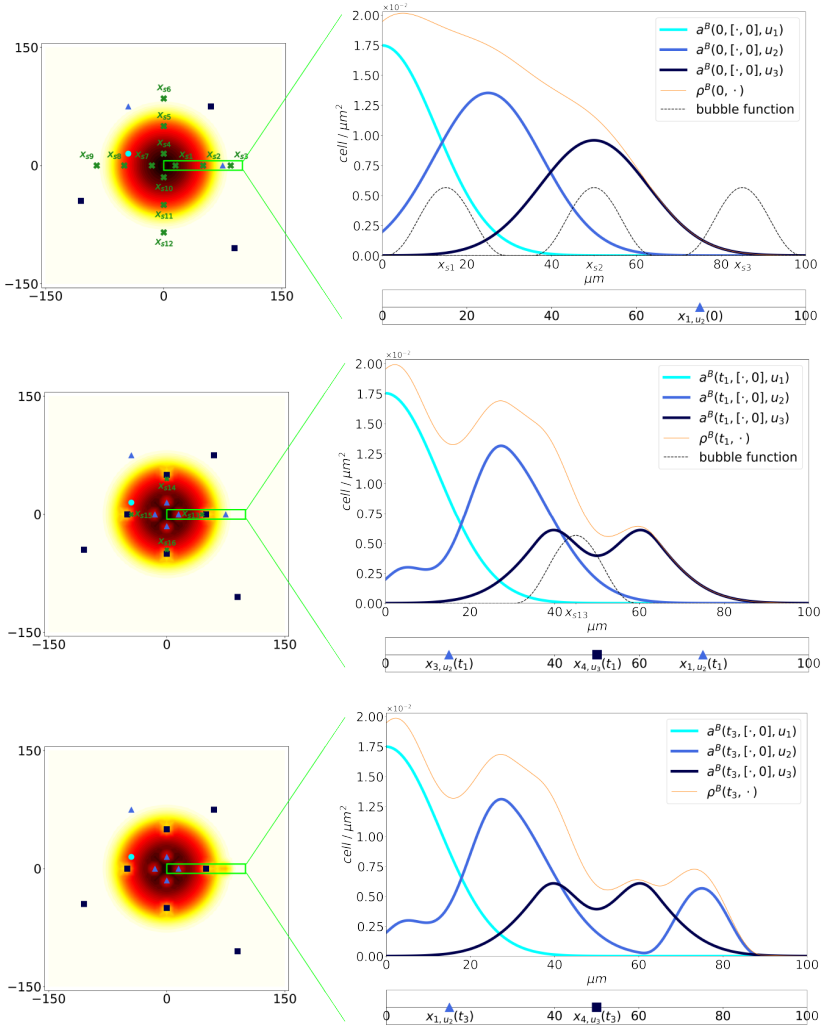

Figure 3: Sample simulation showing how phenotypic switches are implemented in the proposed modeling environment. In the left panels, we represent the evolution of the entire aggregate of cells: in particular, we plot both the overall density of the subpopulation with phenotype B, i.e., ρ^{B} (cf. Eq. (3)), and the set of particles with phenotype A. Within this subgroup, the light blue circles identify cells with genotype u_1, the blue triangles identify cells with genotype u_2, and the dark blue squares identify cells with genotype u_3. The right panels magnificate the dynamics of a representive section of the domain.

The above-described dynamics are schematically visualized, in the case of a representative domain section, in the top-right graph of Fig. 3. The updated

system configuration then reads as[5]

$$\begin{cases} \boldsymbol{X}^{\mathrm{A}}_{u_1}(t_1) = \boldsymbol{X}^{\mathrm{A}}_{u_1}(0); \\ \boldsymbol{X}^{\mathrm{A}}_{u_2}(t_1) = \boldsymbol{X}^{\mathrm{A}}_{u_2}(0) \cup \{\, \boldsymbol{x}_{3,u_2} \equiv \boldsymbol{x}_{\mathrm{s}1}; \boldsymbol{x}_{4,u_2} \equiv \boldsymbol{x}_{\mathrm{s}4}; \boldsymbol{x}_{5,u_2} \equiv \boldsymbol{x}_{\mathrm{s}7}; \boldsymbol{x}_{6,u_2} \equiv \boldsymbol{x}_{\mathrm{s}10} \,\}; \\ \boldsymbol{X}^{\mathrm{A}}_{u_3}(t_1) = \boldsymbol{X}^{\mathrm{A}}_{u_3}(0) \cup \{\, \boldsymbol{x}_{4,u_3} \equiv \boldsymbol{x}_{\mathrm{s}2}; \boldsymbol{x}_{5,u_3} \equiv \boldsymbol{x}_{\mathrm{s}5}; \boldsymbol{x}_{6,u_3} \equiv \boldsymbol{x}_{\mathrm{s}8}; \boldsymbol{x}_{7,u_3} \equiv \boldsymbol{x}_{\mathrm{s}11} \,\}; \\ a^{\mathrm{B}}(t_1, \boldsymbol{y}, u_1) = a^{\mathrm{B}}(0, \boldsymbol{y}, u_1); \\ a^{\mathrm{B}}(t_1, \boldsymbol{y}, u_2) = a^{\mathrm{B}}(0, \boldsymbol{y}, u_2) - \varphi_{\boldsymbol{x}_{\mathrm{s}1}}(\boldsymbol{y}) - \varphi_{\boldsymbol{x}_{\mathrm{s}4}}(\boldsymbol{y}) - \varphi_{\boldsymbol{x}_{\mathrm{s}7}}(\boldsymbol{y}) - \varphi_{\boldsymbol{x}_{\mathrm{s}10}}(\boldsymbol{y}); \\ a^{\mathrm{B}}(t_1, \boldsymbol{y}, u_3) = a^{\mathrm{B}}(0, \boldsymbol{y}, u_3) - \varphi_{\boldsymbol{x}_{\mathrm{s}2}}(\boldsymbol{y}) - \varphi_{\boldsymbol{x}_{\mathrm{s}5}}(\boldsymbol{y}) - \varphi_{\boldsymbol{x}_{\mathrm{s}8}}(\boldsymbol{y}) - \varphi_{\boldsymbol{x}_{\mathrm{s}11}}(\boldsymbol{y}), \end{cases} \tag{13}$$

for all $\boldsymbol{y} \in D$. We indeed have that $N(t_1) = N^{\mathrm{A}}(t_1) + N^{\mathrm{B}}(t_1) = 14 + 180 = 194 = N(0)$.

Successively, at t_2, an analogous local signal is present in the following set of points: $\boldsymbol{x}_{\mathrm{s}13} = (45, 0)$, $\boldsymbol{x}_{\mathrm{s}14} = (0, 45)$, $\boldsymbol{x}_{\mathrm{s}15} = (-45, 0)$, and $\boldsymbol{x}_{\mathrm{s}16} = (0, -45)$, see the central panels in Fig. 3. In all cases, no phenotypic switch actually occurs. In fact, no cell genetic variant has a sufficient amount of mass over the support of $\varphi_{\boldsymbol{x}_{\mathrm{sj}}}$ (with j=13, 14, 15, 16) despite the overall mass of individuals with phenotype B, measured by ρ^{B} would be in principle high enough. In this respect, the system does not vary with respect to (13).

We finally set that at time t_3, the cell $\boldsymbol{x}_{1,u_2}$, located in (75, 0) from the beginning of the observation time, is triggered to turn back to phenotype B, as shown in the bottom panels of Fig. 3. The pointwise particle is indeed replaced by the corresponding bubble function, that is added to the mass of the proper cell genetic variant, as

$$\begin{cases} \boldsymbol{X}^{\mathrm{A}}_{u_1}(t_3) = \boldsymbol{X}^{\mathrm{A}}_{u_1}(t_2) = \boldsymbol{X}^{\mathrm{A}}_{u_1}(t_1) = \boldsymbol{X}^{\mathrm{A}}_{u_1}(0); \\ \boldsymbol{X}^{\mathrm{A}}_{u_2}(t_3) = \boldsymbol{X}^{\mathrm{A}}_{u_2}(t_2) \setminus \{\, \boldsymbol{x}_{1,u_2} \,\} = \boldsymbol{X}^{\mathrm{A}}_{u_2}(t_1) \setminus \{\, \boldsymbol{x}_{1,u_2} \,\}; \\ \boldsymbol{X}^{\mathrm{A}}_{u_3}(t_3) = \boldsymbol{X}^{\mathrm{A}}_{u_3}(t_2) = \boldsymbol{X}^{\mathrm{A}}_{u_3}(t_1); \\ a^{\mathrm{B}}(t_3, \boldsymbol{y}, u_1) = a^{\mathrm{B}}(t_2, \boldsymbol{y}, u_1) = a^{\mathrm{B}}(t_1, \boldsymbol{y}, u_1) = a^{\mathrm{B}}(0, \boldsymbol{y}, u_1); \\ a^{\mathrm{B}}(t_3, \boldsymbol{y}, u_2) = a^{\mathrm{B}}(t_2, \boldsymbol{y}, u_2) + \varphi_{\boldsymbol{x}_{1,u_2}}(\boldsymbol{y}) = a^{\mathrm{B}}(t_1, \boldsymbol{y}, u_2) + \varphi_{\boldsymbol{x}_{1,u_2}}(\boldsymbol{y}); \\ a^{\mathrm{B}}(t_3, \boldsymbol{y}, u_3) = a^{\mathrm{B}}(t_2, \boldsymbol{y}, u_3) = a^{\mathrm{B}}(t_1, \boldsymbol{y}, u_3), \end{cases} \tag{14}$$

for all $\boldsymbol{y} \in D$, so that $N(t_3) = N^{\mathrm{A}}(t_3) + N^{\mathrm{B}}(t_3) = 13 + 181 = 194 = N(0)$. For the sake of reader's convenience, we recall that the element belonging to the set $\boldsymbol{X}^{\mathrm{A}}_{u_2}$ have to be renumbered according to (8).

Remark. As already commented in the Introduction, and sketched in Fig. 1 (C), a cell is stimulated to undergo phenotyic plasticity by environmental signals, but the effective transition depends on its genetic makeup and on the intrinsic stochasticity of the mechanism. These aspects have not been accounted so far, as all the proposed cell phenotypic switches have been set to actually take place

[5] *Notation remark:* since in this simulation setting cell dynamics only include phenotypic plasticity, the differentation between t_i and t_i^+ (for $i = 1, 2, 3$) is not necessary, and therefore avoided for the sake of simplicity.

(provided a sufficient cell mass in the case of B-to-A conversions). Such a model shortcoming is tackled in the next section, where more realistic rules underlying variations in cell phenotype will be given.

3. Model application: early dynamics of an *in vitro* tumor aggregate

We then turn to apply the proposed model to one of the scenarios introduced in Section 1, i.e., the tumor growth. In particular, we hereafter show how our approach can be used to reproduce selected aspects of the early dynamics of a malignant aggregate cultured *in vitro*. In the context of our interest, the trait variable u is set to assume three values, i.e., $U = \{u_1 = 0; u_2 = 0.5; u_3 = 1\}$, each indicating a distinct sequence of genes. In this respect, the higher is the value of u the more the corresponding genotype is associated to cells that in principle have high migratory potential and low proliferation capacity, see Fig. 4 (A). The definition of the structuring variable u is indeed coherent with the "Go or Grow" (GoG) assumption, which finds support from both the experimental [33, 34] and the theoretical literature [35]. Phenotype A, and therefore an individual pointwise representation, is then assigned to describe tumor cells with *mesenchymal* determinants (i.e., that show an effectively high invasiveness and a poor mitotic activity). Phenotype B, as long as a collective density-based representation, is instead assigned to malignant individuals with *epithelial* hallmarks (i.e., low migratory ability but high duplication rates). Such modeling assumptions are sketched in the already-cited panel (A) of Fig. 4.

In agreement with the scheme shown in Fig. 1 (C), we then assume that phenotypic transitions are:

- stimulated by variations in environmental conditions, in particular in the availability of oxygen, whose local concentration will be given by the field variable $O(t, \boldsymbol{y}) : T \times D \mapsto \mathbb{R}_0^+$. In this respect, hypoxia has been widely shown to boost phenotypic instability, acting as a fuel of selective pressure that stimulates tumor cells to shift towards more aggressive (mesenchymal) hallmarks [36]. For instance, tumor cells displaying high levels of hypoxia-inducible factors, such as HIF-1, have been demonstrated to overexpress genes relative to the migratory machinery and underexpress genes related to mitotic processes, see [37] and references therein. In the case of a sufficient amount of resources, malignant individuals have been instead shown to maintain or recover a less invasive (epithelial) behavior. In this respect, cells with low levels of HIF-1 have been shown to transcript mainly genes implicated in duplication activities [37];

- affected by the cell genetic makeup: for instance, a variant characterized by a sequence of genes mainly relative to the migratory machinery more likely maintains or acquires a mesenchymal behavior (and *vice versa*) [38];

- subjected to randomness, which is a critical aspect in most biological phenomena.

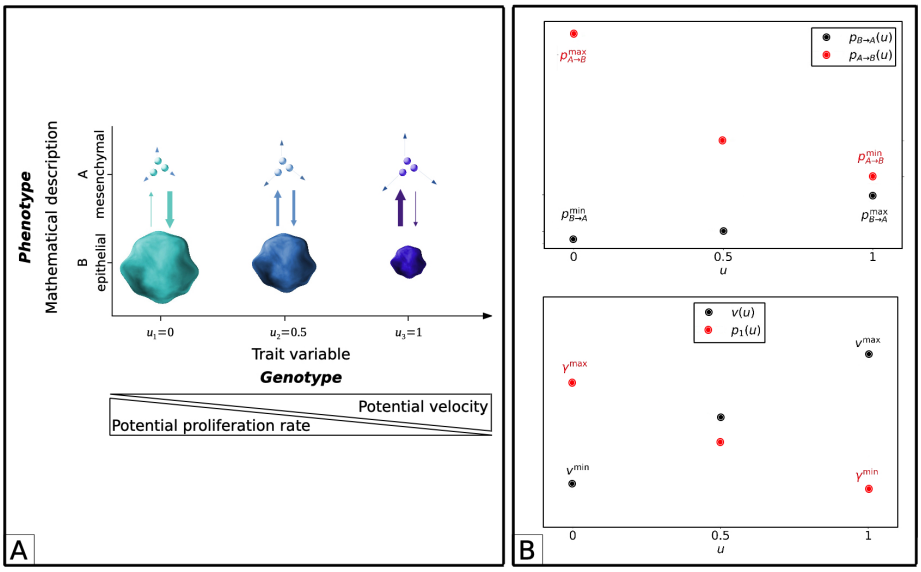

Figure 4: (A) In the proposed model application, the trait value u is set to qualitatively evaluate the cell motility/proliferation potential. In particular, the higher is the value of u the more a tumor individual is assigned a sequence of genes that, if expressed, enhances its migratory ability while dropping its duplication capacity. The phenotype A, and therefore the corresponding pointwise representation, is given to malignant cells with mesenchymal characteristics; the phenotype B, and the corresponding density-based representation, is instead assigned to tumor agents with epithelial hallmarks. The thickness of the vertical arrows gives a qualitative indication of the probability that a cell with a given genotype has to undergo one of the two phenotypic transitions. In particular, as also shown in the bottom graph of the panel (B), cells with genotype $u = u_1 = 0$ more likely acquire (or maintain) an epithelial behavior. In contrast, cells with genotype $u = u_3 = 1$ more likely acquire (or maintain) mesenchymal hallmarks. (B) Top plot: influence of the genetic trait of a cell on the probability of phenotypic conversions (see Eqs. (17) and (20)). Bottom plot: genotypic-dependent duplication rate of malignant epithelial cells (p_1, see Eq. (23)) and speed of mesenchymal individuals (v, see Eq. (27)).

In principle, transition probabilities have to be given as random variables defined on spatio-temporal continuous domains. However, in the perspective of numerical realizations of the proposed model, we here account only for their discretized counterpart. According to these considerations, the probability of a cell $\boldsymbol{x}_{i,u_{\hat{k}}}(t)$ with phenotype A and genotype $u_{\hat{k}} \in U$ to undergo phenotypic transition in an interval of time $(t - \Delta t, t] \subset T$, being Δt the size of the time grid (see below), is equal to:

$$P_{\mathrm{A}\to\mathrm{B}}(O(t, \boldsymbol{x}_{i,u_{\hat{k}}}(t)), u_{\hat{k}}) = q_{\mathrm{A}\to\mathrm{B}}(O(t, \boldsymbol{x}_{i,u_{\hat{k}}}(t)))\; p_{\mathrm{A}\to\mathrm{B}}(u_{\hat{k}}). \tag{15}$$

In (15), the first factor evaluates the environmental conditions experienced by the i-th individual, i.e.,

$$q_{\mathrm{A}\to\mathrm{B}}(O(t, \boldsymbol{x}_{i,u_{\hat{k}}}(t))) = H(O(t, \boldsymbol{x}_{i,u_{\hat{k}}}(t)) - O_{\mathrm{M}}) \tag{16}$$

being

$$H(O(t, \boldsymbol{x}_{i,u_{\hat{k}}}(t)) - O_{\mathrm{M}}) = \left\{1\,,\ \text{if } O(t, \boldsymbol{x}_{i,u_{\hat{k}}}(t)) \geq O_{\mathrm{M}};\ 0\,,\ \text{if } O(t, \boldsymbol{x}_{i,u_{\hat{k}}}(t)) < O_{\mathrm{M}}\right\}$$

the Heaviside function and O_{M} the amount of molecular substance needed by tumor cells to remain in a normoxic condition., i.e., to avoid hypoxia. With Eq. (16), we are assuming that mesenchymal cells experiencing oxygen deprivation do not undergo phenotypic transitions. The second factor in (15) instead reads as:

$$p_{\mathrm{A}\to\mathrm{B}}(u_{\hat{k}}) = (p^{\max}_{\mathrm{A}\to\mathrm{B}} - p^{\min}_{\mathrm{A}\to\mathrm{B}})(1 - u_{\hat{k}})^2 + p^{\min}_{\mathrm{A}\to\mathrm{B}}. \tag{17}$$

It indeed sets a quadratic dependence between the genetic makeup of the cell and its possibility to switch phenotype. In this respect, in the case of normoxic conditions, mesenchymal individuals with genotype $u_1 = 0$ acquire epithelial hallmarks with a probability equal to $p^{\max}_{\mathrm{A}\to\mathrm{B}}$ whereas particles with genotype $u_3 = 1$ with a probability equal to $p^{\min}_{\mathrm{A}\to\mathrm{B}}$ where, according to the above-explained biological arguments, $p^{\min}_{\mathrm{A}\to\mathrm{B}} < p^{\max}_{\mathrm{A}\to\mathrm{B}}$, see Fig. 4 (B-top plot).

Conversely, considering the same time and space discretization of the previous case, a cell clone with genotype $u_{\hat{k}}$ and phenotype B, i.e., whose distribution is given by the density $a^{\mathrm{B}}(t, \cdot, u_{\hat{k}})$, is set to acquire mesenchymal determinants at a certain point $\boldsymbol{x}_{\mathrm{s}} \in D$ of the discretized space and in an interval of time $(t - \Delta t, t] \subset T$ with a probability equal to

$$P_{\mathrm{B}\to\mathrm{A}}(O(t, \boldsymbol{x}_{\mathrm{s}}), u_{\hat{k}}) = q_{\mathrm{B}\to\mathrm{A}}(O(t, \boldsymbol{x}_{\mathrm{s}}))\, p_{\mathrm{B}\to\mathrm{A}}(u_{\hat{k}}), \tag{18}$$

where, recalling (16),

$$q_{\mathrm{B}\to\mathrm{A}}(O(t, \boldsymbol{x}_{\mathrm{s}})) = H(O_{\mathrm{M}} - O(t, \boldsymbol{x}_{\mathrm{s}})). \tag{19}$$

The above formula implies that only hypoxic conditions can trigger epithelial-to-mesenchymal transitions, whose probability to effectively occur depends also in this case by the cell genotype:

$$p_{\mathrm{B}\to\mathrm{A}}(u_{\hat{k}}) = (p^{\max}_{\mathrm{B}\to\mathrm{A}} - p^{\min}_{\mathrm{B}\to\mathrm{A}})u^2_{\hat{k}} + p^{\min}_{\mathrm{B}\to\mathrm{A}}, \tag{20}$$

where $p^{\max}_{\mathrm{B}\to\mathrm{A}}$ characterizes the cell clone with trait $u_3 = 1$ and $p^{\min}_{\mathrm{B}\to\mathrm{A}}$ the cell variant with $u_1 = 0$, being $p^{\max}_{\mathrm{B}\to\mathrm{A}} > p^{\min}_{\mathrm{B}\to\mathrm{A}}$, as plotted in the top graph of Fig. 4 (B). Obviously, the B-to-A phenotypic transition actually takes place if the $u_{\hat{k}}$-th cell variant has enough mass over the support of $\varphi_{\boldsymbol{x}_{\mathrm{s}}}$.

Remarks. For the sake of completeness, we now give some comments on the above-proposed modeling framework:

- as we will see in details in the section devoted to the simulation details, the sizes of the time and space discretization steps affect the estimate of the parameters $p^{\max}_{\mathrm{A}\to\mathrm{B}}, p^{\max}_{\mathrm{A}\to\mathrm{B}}, p^{\max}_{\mathrm{B}\to\mathrm{A}}$ and $p^{\min}_{\mathrm{B}\to\mathrm{A}}$;
- phenotypic transitions are actually employed according to the corresponding procedures explained in the previous section;

- in the case of simultaneously possible epithelial-to-mesenchymal switches occurring in the same domain point, it only takes place the one involving the cell variant with the highest value of u;

- in Eqs. (17) and (20), we have assumed a quadratic relationship between the value of the structuring variable u and the transition probabilities. Different laws may of course be chosen: however, they have to maintain the same qualitative trends of those proposed here;

- more sophisticated functions may be set also to describe the influence of oxygen on phenotypic variations. For instance, the probability of a cell to acquire mesenchymal determinants may increase upon decrements in the chemical concentration below the threshold O_{M}. One could also consider two different oxygen thresholds $O_{\mathrm{M1}} < O_{\mathrm{M2}}$ such that the phenotypic switch from A to B occurs for oxygen concentrations above O_{M1} and the phenotypic switch from B to A occurs for oxygen concentrations below O_{M2}.

Cell dynamics. Malignant cells with epithelial determinants are here assumed to proliferate and undergo random movement. The evolution of the density of the $u_{\hat{k}}$-th variant with phenotype B can be indeed described by means of the following partial differential equation (PDE), whose boundary and initial conditions will be specified later on:

$$\frac{\partial a^{\mathrm{B}}}{\partial t}(t,\boldsymbol{y},u_{\hat{k}}) = \underbrace{D_{\mathrm{B}}\Delta a^{\mathrm{B}}(t,\boldsymbol{y},u_{\hat{k}})}_{\text{diffusive movement}} + \underbrace{p(u_{\hat{k}},\rho(t,\boldsymbol{y}))\, a^{\mathrm{B}}(t,\boldsymbol{y},u_{\hat{k}})}_{\text{proliferation}}, \tag{21}$$

where $\rho(t,\boldsymbol{y})$ account for the local tumor mass (see below Eqs. (25) and (26)). The diffusion term at the r.h.s. of Eq. (21), with constant coefficient $D_{\mathrm{B}} > 0$, models Brownian cell displacements. The reaction term instead expresses local variations in the mass of the $u_{\hat{k}}$-th epithelial cell variant. In particular, they are assumed to depend on (i) individual genetic trait and (ii) physical limitations determined by the available space. In this respect, p can be factorized as it follows:

$$p(u_{\hat{k}},\rho(t,\boldsymbol{y})) = p_1(u_{\hat{k}})\, p_2(\rho(t,\boldsymbol{y})). \tag{22}$$

The duplication law p_1 accounts for the fact that higher proliferation rates characterize cell variants with lower values of the trait variable u (that, as previously seen, are associated to sequence of genes mainly implicated in the mitotic machinery). In this respect, to avoid overcomplications, we assign to p_1 a linear trend, see Fig. 4 (B-bottom plot):

$$p_1(u_{\hat{k}}) = (\gamma^{\max} - \gamma^{\min})(1 - u_{\hat{k}}) + \gamma^{\min}, \tag{23}$$

being $\gamma^{\max}$ a maximal duplication rate, characteristic of cells with genotype $u = u_1 = 0$, and $\gamma^{\min}$ the corresponding minimal value, that is instead assigned to individuals with genotype $u = u_3 = 1$. The factor p_2 in Eq. (22) instead

models the fact that the mitotic cycle is typically disrupted in overcompressed cells, although abnormal proliferation is a relevant characteristic of malignant masses. This phenomenon can be replicated by setting the following logistic law:

$$p_2(\rho(t,\boldsymbol{y})) = 1 - \frac{\rho(t,\boldsymbol{y})}{c}, \tag{24}$$

where $c > 0$ is a carrying capacity while

$$\rho(t,\boldsymbol{y}) = \rho^{\mathrm{A}}(t,\boldsymbol{y}) + \rho^{\mathrm{B}}(t,\boldsymbol{y}), \tag{25}$$

being ρ^{B} defined as in Eq. (3), and

$$\rho^{\mathrm{A}}(t,\boldsymbol{y}) = \sum_{k=1}^{3}\sum_{i=1}^{N_{u_k}^{\mathrm{A}}} \varphi_{\boldsymbol{x}_{i,u_k}(t)}(\boldsymbol{y}). \tag{26}$$

In Eq. (24), we consider that the available space is reduced by the presence also of mesenchymal individuals, whose influence on the overall mass distribution can be accounted by the use of the corresponding set of bubble functions, as given in Eq. (26). Eq. (21) is then equipped by Neumann homogeneous boundary conditions on the spatial domain D, which are consistent with the fact that cells can not physically cross the border of an experimental *Petri dish*.

The dynamics of tumor cells with mesenchymal determinants only include a directional movement towards domain regions with higher oxygen concentrations. In this respect, for the i-th individual with phenotype A and generic genotype $u_{\hat{k}}$, we set:

$$\frac{d\boldsymbol{x}_{i,u_{\hat{k}}}}{dt}(t) = \frac{\nabla O(t,\boldsymbol{x}_{i,u_{\hat{k}}}(t))}{|\nabla O(t,\boldsymbol{x}_{i,u_{\hat{k}}}(t))|}\; v(u_{\hat{k}}), \tag{27}$$

with $v(u_{\hat{k}}) = (v^{\max} - v^{\min})u_{\hat{k}} + v^{\min}$, see the bottom graph in Fig. 4 (B). In Eq. (27), cell speed and direction of movement are decoupled, given their distinct physical meaning. The former depends on the pattern of available resources, the latter, quantified by the scalar functions $v : U \mapsto [v^{\min}, v^{\max}]$, is instead affected by individual genetic makeup. In this respect, recalling that higher values of u imply higher motile potential, $v^{\max}$ is the speed of cells with genotype $u = u_3 = 1$, whereas $v^{\min}$ of cells with genotype $u = u_1 = 0$. It is finally useful to underline that Eq. (27) is based on the *overdamped force-velocity assumption*: it establishes that, in extremely viscous regimes such as biological environments, the velocity of moving agents and not their acceleration is proportional to the sensed forces (see [8] and references therein for a detailed comment). When a mesenchymal cancer cells reaches a point of the border of D, the component of its velocity locally normal to the boundary itself is arbitrarily set equal to zero.

Summing up, it is possible to conclude that, in this sample model application, genetic trait and ecological/environmental conditions not only affect phenotypic

transitions of the cancer cells but also their effective growth and migratory dynamics, as sketched in panel (C) of Fig. 1.

Chemical dynamics. We assume that oxygen diffuses within the domain and is consumed equally by all tumor individuals, regardless their genotype and phenotype. Its kinetics can be therefore described by the following reaction-diffusion (RD) equation:

$$\frac{\partial O}{\partial t}(t,\boldsymbol{y}) = \underbrace{D_{\mathrm{O}}\Delta O(t,\boldsymbol{y})}_{\text{diffusion}} - \underbrace{\lambda_{\mathrm{O}}\,\rho(t,\boldsymbol{y})\,O(t,\boldsymbol{y})}_{\substack{\text{consumption by}\\ \text{tumor cells}}} - \underbrace{\alpha_{\mathrm{O}}O(t,\boldsymbol{y})}_{\text{decay}}, \tag{28}$$

where D_{O}, λ_{O}, and α_{O} are constant coefficients, that quantify chemical diffusion, consumption by malignant cells and natural decay, respectively, being ρ defined as in Eq. (25). Eq. (28) is finally completed with Dirichlet conditions along the entire domain boundary ∂D, i.e., $O(t,\partial D) = \overline{O}$, for all $t \in T$: we are indeed assuming a continuous and constant chemical supply within our virtual *Petri dish*. The oxygen initial pattern will be instead specified below. It is useful to remark that the inclusion of chemical dynamics gives to our model a *multiscale* aspect, as it now deals with elements characteristic of both the cellular and the subcellular levels.

Numerical details. For the spatial domain D, we have employed a triangular mesh with radial simmetry with respect to the center point $(0,0)$. The characteristic diameter of each grid element has been taken equal to $\Delta x = 5\,\mu$m. For the time domain T, we have used an uniform discretization with step equal to $\Delta t = 1$ h.

Eqs. (21) and (28), describing the dynamics of the continuous population and of the oxygen, have been solved employing a time-explicit Euler method coupled with a Galerkin finite-element technique. An explicit Euler method has been also employed for the system of ODEs describing movement of pointwise cells (cf. Eq. (27)). At any discrete time-step, phenotypic switches are implemented (as explained in Section 2) just *after* the numerical solution of the above-cited equation for cell dynamics.

Considering B-to-A switches, the following algorithmic rules are implemented for each numerical node of the domain:

(i) the oxygen level is checked: if it is higher than O_{M}, then no phenotypic transition occurs and we pass to another domain point;

(ii) otherwise, we check the mass of the cell subpopulation with $u = u_3 = 1$: if it satisfies condition (9) then a random number from the uniform distribution between 0 and 1 is drown. If this number is lower than the value of the probability given in (18) and evaluated in the case of our interest, then the phentoypic transition occurs and we pass to another domain point (recall that a B-to-A phenotypic transition of a given subpopulation locally inhibits analogous processes involving other subpopulations);

(iii) otherwise, the same evaluations described at point (ii) are performed for the other subpopulations in descending order with respect to u (to be

coherent with the fact that cells with higher genotypic traits u are more likely to switch phenotype).

We keep into account that, when a B-to-A transition takes place in one point, it affects the possibility of transition in neighboring points, as some of the continuous mass is removed. Thus, in order to avoid biases in spatial location of B-to-A phenotypic switches, at every iteration we randomize the order in which the points of the numerical lattice are visited.

We then turn on considering possible A-to-B transitions, which take place in areas with oxygen concentration above O_{M} with probability given by (15) (using the same drawing algorithm described above). We finally remark that the order in which cells with phenotype A are checked for possible transitions does not affect numerical outcomes, since A-to-B transitions are independent of each other.

All numerical computations have been performed in Fenics, see [39, 40] and references therein.

Parameter estimate. As previously commented, the probabilities of phenotypic transitions introduced in Eqs. (15) and (18) are the discretized approximations of the corresponding continuous-in-time (and in-space) laws. In more details, the coefficient $p^{\max}_{\mathrm{A}\to\mathrm{B}}$ ($p^{\min}_{\mathrm{A}\to\mathrm{B}}$, rsp.) defines the probability that the i-th cell with genotype $u = u_1 = 0$ ($u = u_3 = 1$, rsp.) undergoes phenotypic transition at a given time step, i.e., in the case of normoxic conditions. The estimation of these values is based on the average time that a cell with mesenchymal characteristics takes to re-acquire epithelial hallmarks; in our model we assume that it ranges from $T^{\min}_{\mathrm{A}\to\mathrm{B}} = 50$ h to $T^{\max}_{\mathrm{A}\to\mathrm{B}} = 200$ h. Such quantities (poorly measured in the empirical literature, see [41] for one of the few contributions in this respect) have been fixed in order to have a reasonable number of phenotypic transitions in the period of observation. By recalling that our model is based on the assumption that cells with lower values of the trait variable more likely undergo A-to-B transitions, we can indeed set

$$p^{\max}_{\mathrm{A}\to\mathrm{B}} = \frac{\Delta t}{T^{\min}_{\mathrm{A}\to\mathrm{B}}} \qquad \text{and} \qquad p^{\min}_{\mathrm{A}\to\mathrm{B}} = \frac{\Delta t}{T^{\max}_{\mathrm{A}\to\mathrm{B}}},$$

so that $p^{\max}_{\mathrm{A}\to\mathrm{B}} = 2 \times 10^{-2}$, $p^{\min}_{\mathrm{A}\to\mathrm{B}} = 5 \times 10^{-3}$. The coefficients $p^{\max,\min}_{\mathrm{B}\to\mathrm{A}}$ instead give the probability that a single-cell-fraction of mass with phenotype B and centered in $\boldsymbol{x}_{\mathrm{s}}$ changes phenotype at a given time step when falls in hypoxic conditions. A proper estimate can be obtained by taking into account three aspects: (i) epithelial cells experiencing oxygen deprivation are here assumed to acquire mesenchymal determinants in a time lapse that ranges from $T^{\min}_{\mathrm{B}\to\mathrm{A}} = 8.8$ h to $T^{\max}_{\mathrm{B}\to\mathrm{A}} = 35.4$ h; (ii) in our modeling framework higher values of the genotypic variable imply more possibility to switch towards phenotype A; and (iii) a finer spatial grid requires a smaller transition probability for each node $\boldsymbol{x}_{\mathrm{s}}$, otherwise a higher amount of possible nodes of the domain in principle could allow a higher number of transitions. Taken together, the above considerations lead to

$$p^{\max}_{\mathrm{B}\to\mathrm{A}} \propto \Delta t, (T^{\min}_{\mathrm{B}\to\mathrm{A}})^{-1}, \Delta x^2 \qquad \text{and} \qquad p^{\min}_{\mathrm{B}\to\mathrm{A}} \propto \Delta t, (T^{\max}_{\mathrm{B}\to\mathrm{A}})^{-1}, \Delta x^2.$$

In particular, after preliminary simulations, we have fixed $p^{\max}_{\mathrm{B}\to\mathrm{A}} = 4 \times 10^{-3}$, and $p^{\min}_{\mathrm{B}\to\mathrm{A}} = 10^{-3}$, which have allowed us to have a reasonable rate of B-to-A phenotypic conversions.

The diffusion coefficient of epithelial cell movement, i.e., D_{B}, has been taken equal to $1.29 \times 10^3 \mu\mathrm{m}^2/\mathrm{h}$, as in [42]. The coefficients $\gamma^{\min}$ and $\gamma^{\max}$ quantify the minimal and maximal mitotic rate of cells with phenotype B, in the case of fully available space. The chosen values $\gamma^{\min} = \ln(2)/48\ \mathrm{h}^{-1}$ and $\gamma^{\max} = \ln(2)/24\ \mathrm{h}^{-1}$ fall within the range quantified for glioblastoma cell lines in either hypoxic or normoxic conditions, see again [42]. The carrying capacity c has been set equal to 1.69 cell/$\mu\mathrm{m}^2$, in order to maintain a quasi-monolayered cell configuration, in agreement with the bidimensional nature of experimental cultures in a *Petri dish*.

Cells with phenotype A are allowed to freely move within the domain. In this respect, the maximal value of their speed $v^{\max}$, which characterize mesenchymal individuals with trait $u_3 = 1$ has been fixed to 10 μm/h, whereas the minimal threshold $v^{\min}$, which characterizes mesenchymal individuals with trait $u_1 = 0$, to 2.5 μm/h. These parameters have been taken from [43] and assure that the modulus of the overall cell velocity substantially falls within the range of the corresponding experimental counterparts evaluated for different malignancies.

The chemical threshold that leads to hypoxia, i.e., O_{M}, has been set equal to $2.56 \times 10^{-15}\ \mu\mathrm{mol}/\mu\mathrm{m}^2$, as it is done in [42]. The diffusion coefficient of oxygen has been fixed to $D_{\mathrm{O}} = 3.60 \times 10^6\ \mu\mathrm{m}^2/\mathrm{h}$, and taken again from [42]. The chemical consumption rate then amounts to $\lambda_{\mathrm{O}} = 1.67 \times 10^{-10}\ \mu\mathrm{m}^2/(\mathrm{cell} \cdot \mathrm{h})$: it has been empirically measured taking into account of the proposed computational setup, in order to have a realistic time-evolution of the molecular pattern. The oxygen decay coefficient has been fixed to $\alpha_{\mathrm{O}} = 3.60 \times 10^{-4}\ \mathrm{h}^{-1}$, according to [44]. The constant production of oxygen at the domain border, i.e., $\overline{O}$, has been set equal to $2.8 \times 10^{-15}\ \mu\mathrm{mol}/\mu\mathrm{m}^2$: for the reader's convenience, we remark that this value is $1.1 \times O_{\mathrm{M}}$. The final observation time t_{F} has been instead set equal to 35 h.

The employed parameter setting is listed in Table 1.

Simulation results. The spatial domain D, as well as the initial configuration of the cell system, is exactly the same employed in the representative simulation given in Section 2, specified by Eqs. (11) and (12), and represented in Fig 2. At the onset of the forthcoming numerical realization, we indeed have a tumor aggregate with few mesenchymal cells (heterogenous for genotype) dispersed within and around a cluster of malignant epithelial individuals. In particular, the node of tumor cells with phenotype B has a radial distribution w.r.t. the center of the domain, with the bulk mainly constituted by the cell variant with $u_1 = 0$ and the external region by the cell variant with $u_3 = 1$. The initial oxygen concentration is instead given by the stationary solution of Eq. (28), evaluated in the absence of cancer cells (i.e., in the case only of chemical diffusion and decay): given the low value of the decay rate α_{O} (see above and Table 1), it consists of a spatially quasi-homogeneous pattern with a chemical level approximately equal to $2.8 \times 10^{-15}\ \mu\mathrm{mol}/\mu\mathrm{m}^2$. The initial oxygen level indeed

Parameter	Value [Units]	Reference
r	15 [μm]	[45]
$p^{\min}_{\mathrm{A}\to\mathrm{B}}$	5×10^{-3}	model estimate
$p^{\max}_{\mathrm{A}\to\mathrm{B}}$	2×10^{-2}	model estimate
$p^{\min}_{\mathrm{B}\to\mathrm{A}}$	10^{-3}	model estimate
$p^{\max}_{\mathrm{B}\to\mathrm{A}}$	4×10^{-3}	model estimate
D_{B}	1.29×10^{3} [$\mu\mathrm{m}^2$/h]	[42]
$\gamma_{\min}$	ln(2)/48 [h^{-1}]	[42]
$\gamma_{\max}$	ln(2)/24 [h^{-1}]	[42]
c	1.69 [cell/$\mu\mathrm{m}^2$]	model estimate
$v^{\min}$	2.5 [μm/h]	[43]
$v^{\max}$	10 [μm/h]	[43]
D_{O}	3.60×10^{6} [$\mu\mathrm{m}^2$/h]	[42]
λ_{O}	1.67×10^{-10} [$\mu\mathrm{m}^2/(\mathrm{cell} \cdot \mathrm{h})$]	model estimate
α_{O}	3.60×10^{-4} [h^{-1}]	[44]
O_{M}	2.56×10^{-15} [μmol/$\mu\mathrm{m}^2$]	[42]

Table 1: Simulation parameter setting.

exceeds the hypoxic threshold O_{M} in the entire domain.

Oxygen consumption then starts to occur at the domain area occupied by the tumor aggregate, with the extent of local decrements obviously determined by the density of malignant individuals. The level of chemical at the inner part of the mass indeed drops to the critical value O_{M} and an increasing number of epithelial tumor cells (characterized by negligible motility) experiences hypoxia. Some of them are then able to undergo phenotypic transition and to acquire mesenchymal determinants, see Fig. 5. This group is mainly composed of individuals with a trait value $u_3 = 1$, which is associated to the sequence of genes that favors (from a probabilistic point of view) such a phenotypic switch.

The just-differentiated mesenchymal cells, as long as those already present at the onset of the simulation, crawl towards oxygenated domain regions: in particular, each of them moves with a speed dictated by its genetic trait, as shown by the length of the arrows attached to the particles in Fig. 5. The remaining fraction of epithelial individuals is instead not able to escape harsh environmental conditions: in the case of long-term hypoxia (e.g., long-lasting oxygen deprivation), their fate would be an irreversible necrosis.

As the simulation proceeds, the domain region with low chemical level enlarges: as a result, the above-described cell dynamics take place in more peripheral areas of the tumor aggregate and involves an increasing amount of epithelial mass. In particular, at the end of the observation time (i.e., at $t = t_{\mathrm{F}} = 35$ hours), the cell configuration consists of a hypoxic cluster of epithelial tissue, mainly formed by individuals with a trait variable equal to $u_1 = 0$. It is surrounded by scattered mesenchymal cells, that have reached the external regions of the domain, i.e., those with higher oxygen availability. Interestingly, few of these agents have been able to undergo the inverse transition and reacquire epithelial hallmarks (see the bottom panels of Fig. 5). During the entire obser-

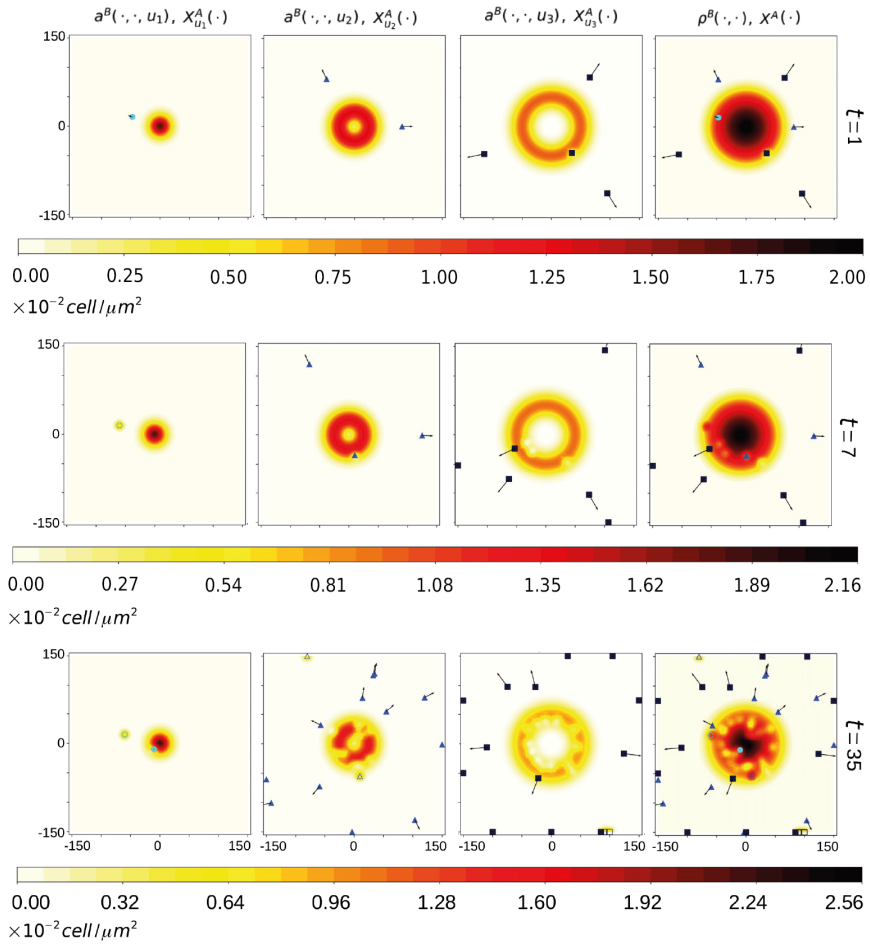

Figure 5: Representative time instants of the evolution of our virtual tumor aggregate. The initial condition of the cell system is exactly the same as in Section 2, see Fig. 2. At the onset of the numerical realization, the oxygen is quasi-homogenously present within the entire domain with a level that is higher than the hypoxic threshold O_{M}. Subsequent oxygen consumption results in harsh conditions for malignant epithelial cells: some of them are then able to acquire mesenchymal hallmarks (according to the genotype-dependent probabilistic rule given in (18)) and move towards domain regions with more availability of resources (see top and middle panels, i.e., those relative to $t = 1$ and 7 h). Arrived close to the border of our virtual *Petri dish*, few of them experience normoxia and recover epithelial determinants (see the bottom panels, i.e., those relative to $t = t_{\mathrm{F}} = 35$ h). We remark that light blue circles identify mesenchymal cells with genotype u_1, blue triangles identify mesenchymal cells with genotype u_2, and dark blue squares identify mesenchymal cells with genotype u_3. The same *empty* geometric labels instead identify mesenchymal cell variants that have undergone the inverse, i.e., A-to-B, phenotypic transition. The arrow attached to each mesenchymal individual identify its velocity: its length is qualitatively proportional to the individual genotype-dependent speed.

vation time, the fraction of malignant epithelial mass goes on proliferating (cf. the variations in the values of the colorbar in Fig. 5).

Our numerical results qualitatively agree with a wide range of experimental evidence, which has shown that malignant cells with different phenotypic properties occupy tumor regions characterised by different oxygen levels. For instance, glioblastoma spheroids cultured *in vitro* have the core mainly populated by cells with a proliferative activity higher than those located at the invasive edges [46, 47, 48, 49]. Analogously, mesenchymal cancer stem cells have been found to be abundant near the tumor-stroma boundary (i.e., at the external region of the malignant mass) [19]. Similar phenotypic spatial heterogeneity has been observed in malignant spheroids of ovarian [50, 51] or breast [52] carcinomas grown in spinner cultures.

Similar growth of tumor masses, i.e., characterized by an inner region of poorly motile individuals unable to escape nutrient deprivation and by an external possibly scattered ring of aggressive cells, has been also predicted by a wide spectrum of theoretical models, see the comprehensive books [53, 54] and the excellent reviews [55, 56, 57, 58, 59].

4. Conclusions and future perspectives

We have here proposed a modeling framework where cells are distinguished in terms of genotype by a discrete structuring variable and in terms of phenotype by the assigned mathematical representation (i.e., pointwise or density-based). A procedure to consistently switch between the two descriptive instances, which is based on the definition and the use of a bubble function, has then allowed to account for phenotypic plasticity.

We have then presented a representative simulation to show how phenotypic transitions actually take place within our theoretical environment, that has been finally applied to a more realistic scenario, i.e., the early evolution of a heterogeneous tumor aggregate hypothetically cultured *in vitro*. In particular, we have assumed that malignant cells can have one of three distinct genotypes and one of two alternative, i.e., mesenchymal vs. epithelial, behavior. Phenotypic conversions have been set to depend on (i) oxygenation levels, (ii) intrinsic genotype, and (iii) randomness, which is a novelty of this work w.r.t. [5, 6]. The resulting numerical realization has captured the realistic emergence of a hypoxic core within the tumor cluster with the consequent cell tendency to acquire a more aggressive and invasive (i.e., mesenchymal) phenotype.

Model improvements. The proposed mathematical environment may be improved at least in two direction.

From a strictly modeling perspective, it would be relevant to account for genetic alterations, that may be induced by cell-cell communication and changes in environmental conditions but that are usually determined by random mutations. This last aspect can be included in the proposed modeling environment by stochastic variations of the value of the trait variable u assigned to one or more pointwise individuals and/or to one or more portions of the cell mass with

the density-based representation. Furthermore, one could consider a continuous trait u that takes values in a given interval (e.g., $[0, 1]$). This would amount in using a structuring variable to represent not only genetic heterogeneity (as in our model), but also epigenetic heterogeneity: each value of u in fact would represent the (normalized) expression of a gene or of a group of genes (or the level of one or more proteins). In this case, epigenetic variations in the cell population could be accounted by including a diffusion term in the trait domain, as done in the already cited works [13, 14, 15].

From an application perspective, our model could be extended to reproduce the evolution of a malignant mass *in vivo*, i.e., to shed lights on the effect of intratumoral heterogeity and phenotypic plasticity on the invasiveness of the disease. In this respect, one may include in the picture the presence of both the preexisting and the tumor-induced vasculature. As a natural extension of our model assumptions, we would in fact have to take into account that cancer cells in hypoxic conditions not only shift towards more aggressive phenotypes but also secrete proangiogenic factors which induce the formation of new blood vessels departing from existing ones [60]. In addition, our model could be developed to incorporate a more comprehensive description of the metabolism of the different cell variants. However, in order to provide consistent results of a such an *in vivo* scenario, model parametrization should be better calibrated, for instance by focusing on a specific tumor type and using proper sets of existing data.

Acknowledgments

This research was partially supported by the Italian Ministry of Education, University and Research (MIUR) through the "Dipartimenti di Eccellenza" Programme (2018-2022) – Dipartimento di Scienze Matematiche "G. L. Lagrange", Politecnico di Torino (CUP: E11G18000350001). All authors are members of GNFM (Gruppo Nazionale per la Fisica Matematica) of INdAM (Istituto Nazionale di Alta Matematica).

References

[1] J. A. Carrillo, M. Fornasier, G. Toscani, F. Vecil, Particle, kinetic, and hydrodynamic models of swarming, in: G. Naldi, L. Pareschi, G. Toscani (Eds.), Mathematical Modeling of Collective Behavior in Socio-Economic and Life Sciences, Modeling and Simulation in Science, Engineering and Technology, Birkäuser, 2010, pp. 297–336.

[2] V. Capasso, D. Morale, Asymptotic behavior of a system of stochastic particles subject to nonlocal interactions, Stochastic Analysis and Applications 27 (3) (2009) 574–603.

[3] D. Drasdo, Coarse graining in simulated cell populations, Advanced Complex Systems 8 (2-3) (2005) 319–363.

[4] K. Bottger, H. Hatzikirou, A. Chauviere, A. Deutsch, Investigation of the migration/proliferation dichotomy and its impact on avascular glioma invasion, Mathematical Modelling Natural Phenomena 7 (1) (2012) 105–135.

[5] A. Colombi, M. Scianna, L. Preziosi, Coherent modelling switch between pointwise and distributed representations of cell aggregates, Journal of mathematical biology 74 (4) (2017) 783–808.

[6] M. Scianna, A. Colombi, A coherent modeling procedure to describe cell activation in biological systems, Communications in Applied and Industrial Mathematics 8 (1) (2017) 1–22.

[7] M. Holzel, A. Bovier, T. Tuting, Plasticity of tumour and immune cells: a source of heterogeneity and a cause for therapy resistance?, Nature Reviews Cancer 13 (5) (2012) 365–376.

[8] M. Scianna, L. Preziosi, Multiscale developments of cellular potts models, Multiscale Modeling & Simulation 10 (2) (2012) 342–382.

[9] A. R. A. Anderson, A. M. Weaver, P. T. Cummings, V. Quaranta, Tumor morphology and phenotypic evolution driven by selective pressure from the microenvironment, Cell 127 (5) (2006) 905–915.

[10] C. Giverso, T. Lorenzi, L. Preziosi, Effective interface conditions for continuum mechanical models describing the invasion of multiple cell populations through thin membranes, Applied Mathematics Letters 125 (107708) (2022) 1–9.

[11] S. M. Wise, J. S. Lowengrub, H. B. Frieboes, V. Cristini, Three-dimensional multispecies nonlinear tumor growth— I Model and numerical method, Journal of Theoretical Biology 253 (3) (2008) 524–543.

[12] H. N. Weerasinghe, P. M. Burrage, K. Burrage, D. V. Nicolau, Mathematical models of cancer cell plasticity, Journal of Oncology 2019 (2019) 1–14.

[13] G. Fiandaca, M. Delitala, T. Lorenzi, A mathematical study of the influence of hypoxia and acidity on the evolutionary dynamics of cancer, Bulletin of mathematical biology 83 (83) (2021) 1–29.

[14] T. Lorenzi, C. Venkataraman, A. Lorz, M. A. J. Chaplain, The role of spatial variations of abiotic factors in mediating intratumour phenotypic heterogeneity, Journal of theoretical biology 451 (2018) 101–110.

[15] A. Lorz, T. Lorenzi, J. Clairambault, A. Escargueil, B. Perthame, Modeling the effects of space structure and combination therapies on phenotypic heterogeneity and drug resistance in solid tumors, Bulletin of mathematical biology 77 (1) (2015) 1–22.

[16] O. Ilina, P. Friedl, Mechanisms of collective cell migration at a glance, Journal of Cell Science 122 (18) (2009) 3203–3208.

[17] A. A. Khalil, P. Friedl, Determinants of leader cells in collective cell migration, Integrative Biology 2 (11-12) (2010) 568–574.

[18] M. Boareto, M. K. Jolly, A. Goldman, P. M., S. A. Mani, S. Sengupta, B.-J. Eshel, L. Herbert, N. O. Jose', Notch-jagged signalling can give rise to clusters of cells exhibiting a hybrid epithelial/mesenchymal phenotype, Journal of the Royal Society Interface 13 (118) (2016) 1–11.

[19] S. Liu, Y. Cong, D. Wang, Y. Sun, L. Deng, Y. Liu, R. Martin-Trevino, L. Shang, S. P. McDermott, M. D. Landis, S. Hong, A. Adams, R. D'Angelo, C. Ginestier, E. Charafe-Jauffret, S. G. Clouthier, D. Birnbaum, W. S. T., M. Zhan, J. C. Chang, M. S. Wicha, Breast cancer stem cells transition between epithelial and mesenchymal states reflective of their normal counterparts, Stem Cell Reports 2 (1) (2013) 78–91.

[20] C. K. Williams, J. L. Li, M. Murga, A. L. Harris, G. Tosato, Upregulation of the notch ligand delta-like inhibits vegf induced endothelial cell function, Blood 107 (3) (2006) 931–939.

[21] M. Al-Hajj, M. S. Wicha, A. Benito-Hernandez, S. J. Morrison, M. F. Clarke, Prospective identification of tumorigenic breast cancer cells, Proceedings of the National Academy of Sciences 100 (7) (2003) 3983–3988.

[22] C. A. O'Brien, A. Pollett, S. Gallinger, J. E. Dick, A human colon cancer cell capable of initiating tumour growth in immunodeficient mice, Nature 445 (7123) (2007) 106–110.

[23] S. K. Singh, C. Hawkins, I. D. Clarke, J. A. Squire, J. Bayani, T. Hide, R. M. Henkelman, M. D. Cusimano, P. B. Dirks, Identification of human brain tumour initiating cells, Nature 432 (7015) (2004) 396–401.

[24] A. T. Collins, P. A. Berry, C. Hyde, M. J. Stower, N. J. Maitland, Prospective identification of tumorigenic prostate cancer stem cells, Cancer Research 65 (23) (2005) 10946–10951.

[25] A. Marusyk, V. Almendro, K. Polyak, Intra-tumour heterogeneity: a looking glass for cancer?, Nature Reviews Cancer 12 (2012) 323–334.

[26] M. A. Nieto, R. Y.-J. Huang, R. A. Jackson, J. P. Thiery, Emt: 2016, Cell 166 (1) (2016) 21–45.

[27] A. Roesch, Tumor heterogeneity and plasticity as elusive drivers for resistance to mapk pathway inhibition in melanoma, Oncogene 34 (23) (2015) 2951–2957.

[28] J. Varga, T. De Oliveira, F. R. Greten, The architect who never sleeps: tumor-induced plasticity, FEBS Letters 588 (15) (2014) 2422–2427.

[29] M. D. Brooks, M. L. Burness, M. S. Wicha, Therapeutic implications of cellular heterogeneity and plasticity in breast cancer, Cell Stem Cell 17 (3) (2015) 260–271.

[30] S. M. Mooney, M. K. Jolly, H. Levine, P. Kulkarni, Phenotypic plasticity in prostate cancer: role of intrinsically disordered proteins, Asian Journal of Andrology 18 (5) (2016) 704–710.

[31] A. Colombi, M. Scianna, A. Tosin, Differentiated cell behaviour: a multiscale approach using measure theory, Journal of Mathematical Biology 71 (5) (2014) 1049–1079.

[32] A. Colombi, M. Scianna, L. Preziosi, A measure-theoretic model for cell migration and aggregation, Mathematical Modelling of Natural Phenomena 10 (1) (2015) 4–35.

[33] A. Giese, L. Kluwe, M. E. Berens, M. Westphal, Migration of human glioma cells on myelin, Neurosurgery 38 (4) (1996) 755–764.

[34] A. Giese, M. A. Loo, N. Tran, D. Haskett, S. W. Coons, M. E. Berens, Dichotomy of astrocytoma migration and proliferation, Int. J. Cancer 67 (2) (1996) 275–282.

[35] S. M. Schaller, A. Deutsch, H. Hatzikirou, D. Basanta, 'Go or grow': the key to the emergence of invasion in tumour progression?, Mathematical Medicine and Biology 29 (1) (2012) 49–65.

[36] S.-H. Kao, K.-J. Wu, W.-H. Lee, Hypoxia, epithelial-mesenchymal transition, and tet-mediated epigenetic changes, Journal of Clinical Medicine 5 (2) (2016) 24–38.

[37] H. N. Barrak, A. K. Maitham, Y. A. Luqmani, Hypoxic environment may enhance migration/penetration of endocrine resistant mcf7-derived breast cancer cells through monolayers of other non-invasive cancer cells in vitro, Scientific Reports 10 (1) (2020) 1–14.

[38] H. L. Rocha, I. Godet, F. Kurtoglu, J. Metzcar, K. Konstantinopoulos, S. Bhoyar, D. M. Gilkes, P. Macklin, A persistent invasive phenotype in post-hypoxic tumor cells is revealed by fate mapping and computational modeling, Science 24 (9) (2021) 1–22.

[39] M. S. Alnaes, J. Blechta, J. Hake, A. Johansson, B. Kehlet, A. . Logg, A. Richardson, J. Ring, M. E. Rognes, G. N. Wells, The fenics project version 1.5, Archive of Numerical Software 3 (100) (2015) 9–23.

[40] A. Logg, K.-A. Mardal, G. N. Wells, Automated Solution of Differential Equations by the Finite Element Method, Springer, 2012.

[41] N. M. Aiello, R. Maddipati, R. J. Norgard, D. Balli, J. Li, S. Yuan, T. Yamazoe, T. Black, A. Sahmoud, E. E. Furth, D. Bar-Sagi, B. Z. Stanger, Emt subtype influences epithelial plasticity andmode of cell migration, Developmental Cell 45 (2018) 681–695.

[42] A. Martínez-González, G. F. Calvo, L. A. Pérez Romasanta, V. Pérez-García, Hypoxic cell waves around necrotic cores in glioblastoma: a biomathematical model and its therapeutic implications, Bulletin of Mathematical Biology 74 (12) (2012) 2875–2896.

[43] J. A. Gallaher, J. S. Brown, A. R. A. Anderson, The impact of proliferation-migration tradeoffs on phenotypic evolution in cancer, Scientific Reports 9 (2425) (2019) 1–10.

[44] P. Cumsille, A. Coronel, C. Conca, C. Quiñinao, C. Escudero, Proposal of a hybrid approach for tumor progression and tumor-induced angiogenesis, Theoretical Biology and Medical Modelling 12 (13) (2015) 1–22.

[45] B. Alberts, A. Johnson, J. Lewis, Molecular Biology of the Cell 4th edition, Garland Science, 2002.

[46] R. Abramovitch, G. Meir, M. Neeman, Neovascularization induced growth of implanted c6 glioma multicellular spheroids: magnetic-resonance microimaging, Cancer Research 55 (9) (1995) 1956–1962.

[47] M. A. A. Castro, F. Klamt, V. A. Grieneisen, I. Grivicich, J. C. F. Moreira, Gompertzian growth pattern correlated with phenotypic organization of colon carcinoma, malignant glioma and non-small cell lung carcinoma cell line, Cell Proliferation 36 (2) (2003) 65–73.

[48] D. Khaitan, S. Chandna, M. B. Arya, D. B. S., Establishment and characterization of multicellular spheroids from a human glioma cell line: implications for tumor therapy, J. Transl. Med. 4 (12) (2006) 1–13.

[49] A. M. Stein, T. Demuth, D. Mobley, M. Berens, L. M. Sander, A mathematical model of glioblastoma tumor spheroid invasion in a three-dimensional in vitro experiment, Biophysical Journal 92 (1) (2007) 356–365.

[50] K. M. Burleson, M. P. Boente, S. E. Parmabuccian, A. P. Skubitz, Disaggregation and invasion of ovarian carcinoma ascites spheroids, Journal of Translational Medicine 4 (6) (2006) 1–16.

[51] K. Shield, M. L. Ackland, N. Ahnmed, G. E. Rice, Multicellular spheroids in ovarian cancer metastases: biology and pathology, Gynecologic Oncology 113 (1) (2009) 143–148.

[52] R. A. Gatenby, K. Smallbone, P. K. Maini, F. Rose, J. Averill, R. B. Nagle, L. Worrall, R. J. Gillies, Cellular adaptations to hypoxia and acidosis during somatic evolution of breast cancer, British Journal of Cancer 97 (5) (2007) 646–653.

[53] V. Cristini, J. Lowengrub, Multiscale modeling of cancer: An integrated experimental and mathematical modeling approach, Cambridge University Press, 2010.

[54] L. Preziosi, Cancer modelling and simulation, CRC Press, 2003.

[55] R. P. Araujo, D. L. S. McElwain, A history of the study of solid tumour growth: the contribution of mathematical modelling, Bulletin of Mathematical Biology 66 (2004) 1039–1091.

[56] N. Bellomo, N. K. Li, P. K. Maini, On the foundations of cancer modelling: selected topics, speculations, and perspectives, Mathematical Models and Methods in Applied Sciences 18 (04) (2008) 593–646.

[57] H. M. Byrne, T. Alarcon, M. R. Owen, S. D. Webb, P. K. Maini, Modelling aspects of cancer dynamics: a review, Philosophical Transactions of the Royal Society A: Mathematical, Physical and Engineering Sciences 364 (1843) (2006) 1563–1578.

[58] M. A. Chaplain, Avascular growth, angiogenesis and vascular growth in solid tumours: The mathematical modelling of the stages of tumour development, Mathematical and Computer Modelling 23 (6) (1996) 47–87.

[59] V. Quaranta, A. M. Weaver, P. T. Cummings, A. R. A. Anderson, Mathematical modeling of cancer: the future of prognosis and treatment, Clinica Chimica Acta 357 (2) (2005) 173–179.

[60] K. H. Plate, G. Breier, H. A. Weich, W. Risau, Vascular endothelial growth factor is a potential tumour angiogenesis factor in human gliomas in vivo, Nature 359 (6398) (1992) 845–848.